Applied Catalysis B: Environmental 205 (2017) 624–630

Contents lists available at ScienceDirect

Applied Catalysis B: Environmental

journal homepage: www.elsevier.com/locate/apcatb

Facile fabrication of high-yield graphitic carbon nitride with a large surface area using bifunctional urea for enhanced photocatalytic performance

Xue Lu Wang, Hua Gui Yang*

Key Laboratory for Ultrafine Materials of Ministry of Education, School of Materials Science and Engineering, East China University of Science and Technology, 130 Meilong Road, Shanghai 200237, China

ARTICLE INFO

Article history:
Received 27 October 2016
Received in revised form
27 December 2016
Accepted 4 January 2017
Available online 4 January 2017

Keywords:
Photocatalysis
Graphitic carbon nitride
Hydrogen evolution
High-yield
Bifunctional

ABSTRACT

Graphitic carbon nitride ($g\text{-}C_3N_4$) has aroused intense expectations owing to its outstanding visible-light-response capability for hydrogen generation from water. However, the low-yield, low practical surface area and high photogenerated charge recombination rate severely limits its photocatalytic performance. Here, in this study high-yield synthesis of $g\text{-}C_3N_4$ with a large surface area has been achieved successfully through an in situ pyrolysis of cyanamide with the assist of the bifunctional urea. During the synthesis process, urea may decompose into a lot of ammonia and carbon dioxide, which acts as the supplementary-nitrogen-source and bubble-generating template respectively. It is found that the surface area and photocatalytic activity can be controlled by adjusting the addition of the environmentally friendly bifunctional urea. The as-prepared $g\text{-}C_3N_4$ exhibits unique optical activity as well as photoelectriochemical activity for solar-to-chemical conversion, and this simple bifunctional method may open a new pathway for designing and optimizing of photocatalysts.

© 2017 Elsevier B.V. All rights reserved.

1. Introduction

Utilization of renewable and clean energy resources and development of eco-friendly practical systems for environmental remediation have evoked much attention owing to the decline in fossil-fuel production and increasing concern on environmental issues [1–4]. In particular, photocatalytic water splitting using photocatalysts represents a highly attractive way to convert solar energy, which is the most abundant and universally available source of renewable energy, into hydrogen that is considered as an ideal fuel for future energy sustainability [5–8]. Therefore, searching and optimizing highly efficient photocatalysts for photocatalytic hydrogen evolution reaction (HER) is of great significance. Amongst all existing semiconductor photocatalysts being thermodynamically capable of HER, graphitic carbon nitride ($g\text{-}C_3N_4$) has stimulated particular interests because of its high in-plane nitrogen content, excellent chemical and thermal stability, and appealing electronic structure [9–15]. Unfortunately, the low specific surface area, low-yield and insufficient solar-light absorption severely limit the photocatalytic performance of conventional bulk $g\text{-}C_3N_4$ [16–19]. In this context, considerable and continuing effort has been devoted to improve the activity of $g\text{-}C_3N_4$ based photocatalysts.

To improve the photocatalytic performance of $g\text{-}C_3N_4$, several strategies, such as nanostructuring [20–22], doping [23–25], cocatalyzing [26–28], copolymerization [29–31] and exfoliation [32–34], have been exploited. The high-yield synthesis of $g\text{-}C_3N_4$ with high surface area is of particular interest because a larger surface area can be favourable for photocatalytic reaction by providing more surface reactive sites and increasing the mass transfer [18,35]. Generally, $g\text{-}C_3N_4$ with a large surface area is obtained by a template-induced method. One is the “hard template” method [36,37]. By utilizing this method, the surface areas can be controlled by different silica or anodic aluminium oxides templates. However, the removal of the host matrices by aqueous ammonium bifluoride or hydrogen fluoride may result in some impurity residues, and the removal process is also complex and time-consuming [17,32]. The other is the “soft-template” method, but this method may result in some carbon residue and nitride loss [38–40]. Besides, the commonly used one-step method for the bulk $g\text{-}C_3N_4$ preparation suffers from a very low yield(~6%), because the polymerization temperature is higher than the sublimation point of the reagent and the gas intermediate product (ammonia) is also participate in the later polymerization [41]. Hence, it is of great urgency to develop a

* Corresponding author.
E-mail address: hgyang@ecust.edu.cn (H.G. Yang).

http://dx.doi.org/10.1016/j.apcatb.2017.01.013
0926-3373/© 2017 Elsevier B.V. All rights reserved.

facile and economic synthesis method of high-yield g-C_3N_4 with a large surface area for the industrial and practical applications.

Here, we demonstrated an efficient method that high-yield g-C_3N_4 with a large surface area can be developed by in situ direct pyrolysis of cyanamide with the assist of the bifunctional urea. The dissolution of the urea into the molten cyanamide at the temperature of 60 °C can result in the formation of intermolecular hydrogen bonds network. During the synthesis process of g-C_3N_4, urea may decompose into a lot of ammonia (NH_3) and carbon dioxide (CO_2), which serves as the nitrogen-source supply and the bubble-generating template respectively. Since the hydrogen bonds network can suppress the escape of the NH_3, a high yield (60–70%) production of g-C_3N_4 is achieved. The surface area structure and photocatalytic activity can be easily controlled by adjusting the mass ratio of urea to cyanamide. The resultant g-C_3N_4 provides a large accessible surface area, and exhibits significantly improved optical and electronic properties.

2. Experimental

2.1. Synthesis of photocatalysts

Typically, 2 g of the different mass ratios of cyanamide and urea powders were added into a covered crucible, and then the mixture was heated in an oil bath at 60 °C for 30 min. After it turned into the molten state, the crucible was then taken out from the oil bath to cool down to the room temperature. Then, the resultant powders were calcined at 550 °C for 2 h in air, and the final samples were obtained. According to the mass content of urea, the as-prepared samples were named as CN, CN-0.5, CN-1, CN-1.5 and CN-2, respectively.

2.2. Material characterization

The structures of the powder samples were investigated by X-ray diffactometer (XRD, Bruker D8 Advanced Diffactometer operating with Cu Kα radiation). The angular range was 2θ = 5–55°, with a speed of 6°/min. Infrared transmission was obtained with a Fourier transform infrared (FTIR) spectrophotometer Spectrum (Nicolet). The optical absorbance spectra of the samples were performed on using a UV–vis spectrometer (CARY 300). Element analysis (EA) was conducted by an elemental analyzer (vario ELII; Elementar Analysensyteme, Germany). The photoluminescence (PL) measurements were performed in an Edinburgh instruments (FLSP 920) system operated at room temperature. Brunauer-Emmett Teller (BET) surface areas were determined by a TriStar 3020 nitrogen sorption isotherm apparatus. Transmission electron mictoscopy (TEM, JEM 2100, 200 kV) were used to characterize the morphology and structure of the obtained products.

2.3. Photocatalytic experiments

The photocatalytic reaction was performed in a pyrex glass cell connected to a glass closed gas circulation system. The deposition of 3 wt% Pt was conducted by direactly immersing the products into H_2PtCl_6 ethanol solution and calacinated at 180 °C for 30 min (ramp: 2 °C min^{-1}). H_2 evolution analysis was performed by dispersing 50 mg of catalyst powder in an aqueous solution containing triethanolamine (100 mL, 10 vol.%) as the sacrificial electron donor. The reactant solution was evacuated several times to remove air completely before the reaction. A 300 W Xe lamp with a 420 nm cutoff filter was used as the light source. A flow of cooling water was used during the reaction to maintain the temperature of the reactant solution at 15 °C. The amount of evolved H_2 evolved was analyzed by gas chromatography (TECHCOMP, 7890 II).

2.4. Photoelectrochemical measurements

Photocurrent was conducted with an electrochemical analyzer (CHI660E Instruments) in a standard three-electrode system using the prepared samples as the working electrodes, using a Pt gauze electrode and Ag/AgCl (saturated KCl) as the counter electrode and reference electrode, respectively. The working electrodes were immersed in the electrolyte (0.2 M Na_2SO_4 aqueous solution) for 60 s before any measurements were taken.

The working electrode was prepared on fluoride tin oxide (FTO) conductor glass, which was cleaned by sonication in acetone and ethanol for 10 min each. 10 mg of powder was mixed with 0.2 mL DMF and 0.05 mL Liquion solution to make a slurry. The slurry was then injected onto the FTO glass, whose sides were previously covered with Scotch tape and the exposed area of electrodes was 0.785 cm^2. These electrodes were dried at 120 °C for 30 min in air to improve adhesion.

3. Results and discussion

Cyanamide is an organic precursor with a low melting point, usually below 50 °C. When the mixture of cyanamide and urea was heated in an oil bath at 60 °C for 30 min, the urea would dissolve into the molten cyanamide and the intermolecular hydrogen bonds network might formed on account of the existence of the electronegative atoms such as nitrogen and oxygen [42,43]. For a better understanding of the different reaction processes of CN-x samples, thermogravimetric analysis (TGA) was carried out. All the precursors were heated from room temperature to 1000 °C at a rate of 10 °C min^{-1} in air, and the TGA curves are shown in Fig. 1. As evidenced by TGA, the addition of urea might obviously increase the 2nd stage reaction time between 200 °C to 400 °C, indicating that partial generated NH_3 re-participate in the pyrolysis process due to the hydrogen bonds network. Fig. 2 shows the TEM image of as-synthesized CN, CN-1.5 and CN-2 samples. A layered and plate-like surface morphology consisting of winkles is exhibited on CN-1.5. Some breakage of the plate which is induced by the bubble templates can be found, which make the CN-1.5 possess a large specific surface area. As can be seen from the N_2 adsorption-desorption isotherms of the as-prepared CN-x samples (Fig. 3), the surface area of CN-1.5 was about 59.9 m^2 g^{-1}, more than five times larger than CN which is synthesized without the assist of urea. This indicates that CO_2 gas generated from the pyrolysis of urea can act as the bubble template.

The structure of the as-prepared samples was detected by XRD. All XRD patterns in Fig. 4a exhibit two distinct peaks at round 27.4°

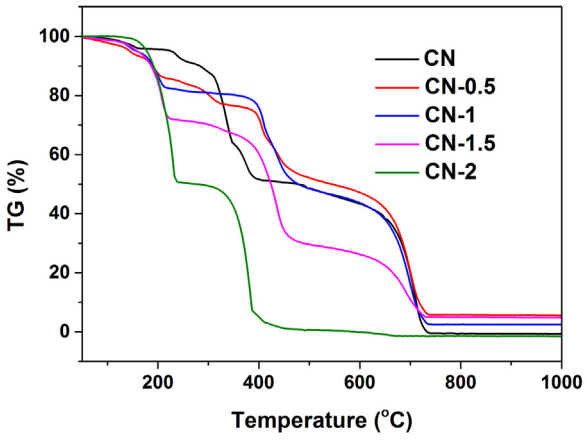

Fig 1. Thermogravimetric analysis (TGA) curves of CN and CN-x (x = 0.5, 1, 1.5 and 2) samples.

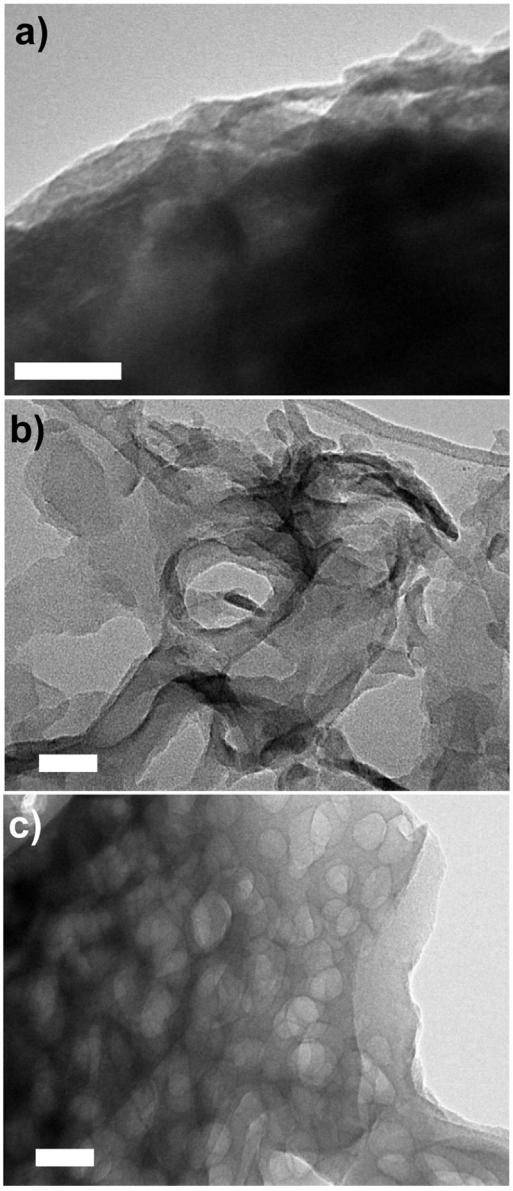

Fig. 2. TEM images of (a) CN, (b) CN-1.5 and (c) CN-2 samples. Scale bar is 50 nm.

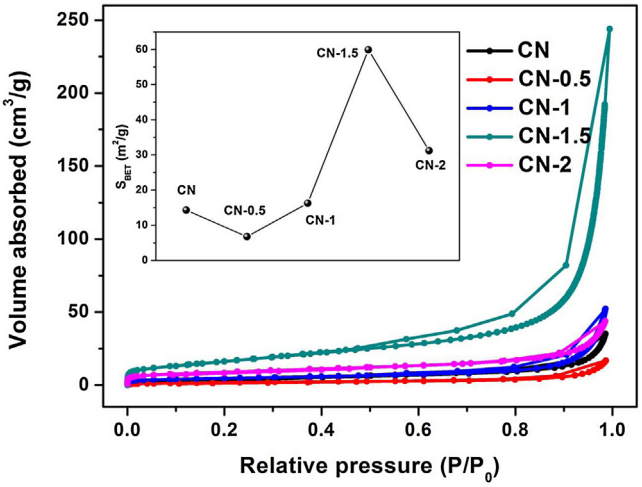

Fig. 3. N_2 adsorption-desorption isotherms of CN and CN-x (x = 0.5, 1, 1.5 and 2) samples.

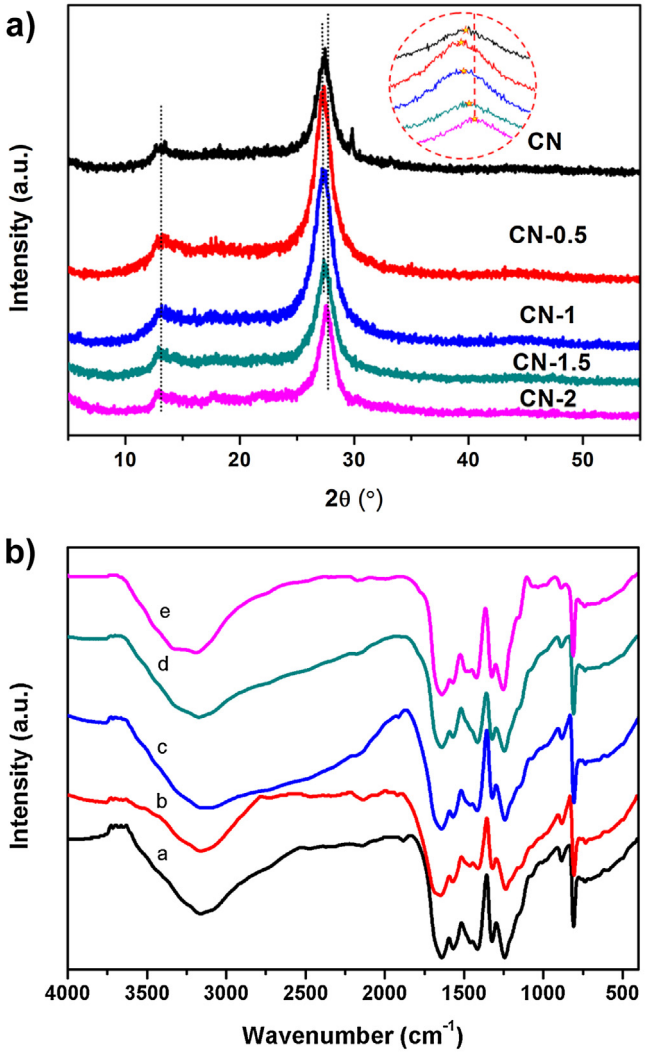

Fig. 4. (a) X-ray diffraction (XRD) patterns of CN and CN-x samples. (b) Fourier transform infrared spectra (FTIR) of CN (a), CN-0.5 (b), CN-1 (c), CN-1.5 (d) and CN-2 (e) samples.

and 13.1°, corresponding to the interlayer stacking reflection of conjugated aromatic systems and the inplane structural repeating motif, respectively. The similarity of XRD patterns indicates that the addition of urea has no significant influence on the graphitic stacking structures of g-C_3N_4. However, the peak (002) of CN-x slightly down-shift at first and then up-shift; that is, the average interlayer distance of the CN-x is notably loosened for the CN-0.5 and compressed gradually from CN-1 to CN-2 [44,45].

Fig. 4b shows the FTIR spectra of the CN-x samples. All the samples show the feature-distinctive stretch modes of aromatic CN heterocycles at 1200–1700 cm^{-1} together with the breathing mode of the triazine units at around 810 cm^{-1}, which is very similar to that of g-C_3N_4. The broad bands in the range of 3000–3500 cm^{-1} were attributed to the adsorbed H_2O bands and N—H components [46,47].

The element contents were further confirmed by elemental analyses (Table 1). According to the EA results, the C/N molar ratio of CN and CN-2 samples are 0.672 and 0.681, respectively; this ratio slightly decreases for the CN-0.5, CN-1 and CN-1.5 samples compared with CN. It's worth noting that all CN-x products with the addition of urea have a perfect nitrogen content (~58% in weight), which are much higher than that of the CN and CN-2 samples. This is an indication that the generated NH_3 incorporated in the syn-

Table 1
The results of elemental analysis for the CN and CN-x (X = 0.5, 1, 1.5 and 2) samples.

Sample	N [wt%]	C (wt%)	H (wt%)	Atom ratio (C/N)
CN	54.80	31.55	2.79	0.672
CN-0.5	58.09	33.25	2.51	0.668
CN-1	58.59	33.58	2.35	0.669
CN-1.5	58.21	33.49	2.39	0.671
CN-2	57.85	33.77	2.41	0.681

thesis of g-C_3N_4 which is caused by the formed hydrogen bonds network, resulting the high yield g-C_3N_4 with the synergistic effect of the cyanamide and urea.

The optical properties of the CN-x products were studied by recording UV–vis (UV–vis) absorption spectra and photoluminescence (PL) spectra. Fig. 5a shows the UV–vis spectra of the five samples. The involvement of both the urea might modify the π-electron delocalization in the conjugated system, and thus changes the intrinsic optical/electronic properties of the CN-x samples. With increasing the ratio of the urea, a remarkable red shift of the optical absorption was observed at first, owing to the extension of electron delocalization in the aromatic sheets with enhanced structural connections, somewhat similar to the bathochromic shift effect in J-aggregates [48,49]. Subsequently, it indeed shifts to a shorter wavelength compared with CN. The hypsochromic-shift performance of CN-1.5 and CN-2 are presumably due to the strong quantum confinement effects, because of the enhanced surface area. As for the band gap, a gradually increased tendency can be inspected from 2.70 eV of the CN to 2.92 eV of the CN-2 (Fig. 5b). To our knowledge, the enlarged band gap, along with the enhanced surface area are favourable for light-harvesting, charge transfer and mass-transport and should in principle alter the photocatalytic properties of carbon nitride significantly.

The increasing bandgaps from CN to CN-2 can be further confirmed by the gradually blue shift of the fluorescence emission (Fig. 6) which is originated from the recombination of free charge carriers. This might be ascribed to the quantum confinement effect by shifting the conduction and valence band edges in opposite directions. It was remarkable that an obvious fluorescence quenching is observed for CN-0.5, CN-1 and CN-1.5, and CN-1.5 is the lowest among all the CN and CN-x samples, possibly indicating the

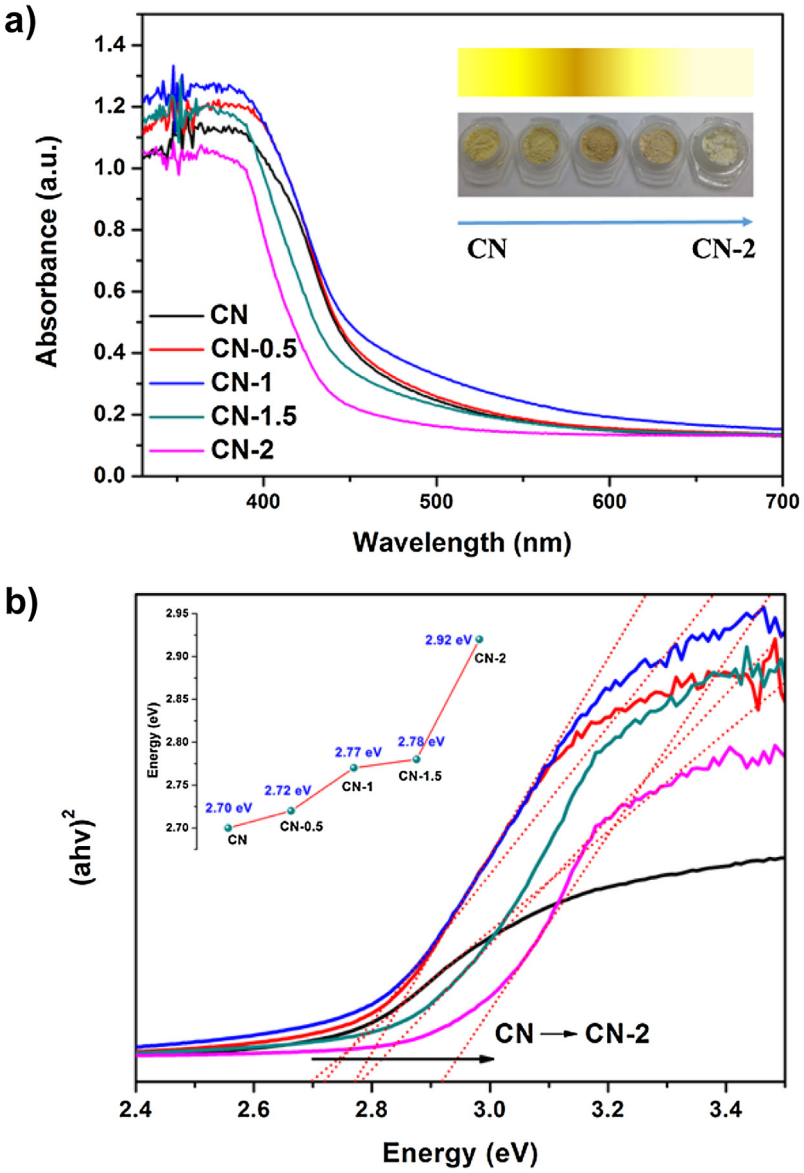

Fig. 5. (a) Optical properties of the samples. (a) UV–vis absorption spectra and the (b) band gaps of the CN and CN-x (x = 0.5, 1, 1.5 and 2) samples.

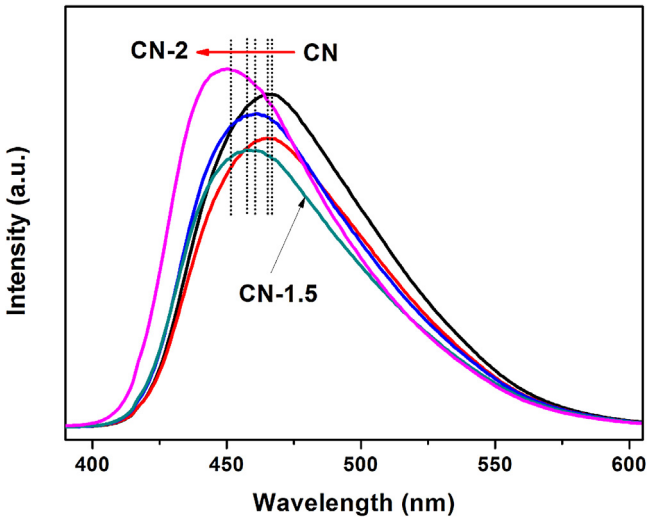

Fig. 6. Photoluminescence emission spectra of CN and CN-x samples.

electron delocalization on surface terminal sites, or the reduced density of charge carrier traps for electron-hole recombination in CN-1.5.

Visible-light-induced H_2 production was investigated to examine the catalytic activity of the CN and CN-x samples by using 3 wt% Pt as the cocatalyst. As shown in Fig. 7a, all the CN-x samples with the assist of urea (CN-0.5, CN-1 and CN-1.5) demonstrate an enhanced hydrogen evolution rate (HER) over CN and CN-2, and the best sample CN-1.5 experts 10 and 5 times higher performance than CN and CN-5 respectively.

The effect of the incident light with different wavelength on the photocatalytic activity was shown in Fig. 7b. Seven kinds of band-pass filters (365, 380, 420, 450, 500, 520 and 550 nm) were used. The H_2 evolution rates mostly agree well with the diffuse reflectance spectra, indicating that the reaction is indeed driven by light absorption on the catalyst. Note that the rate of H_2 production under the irradiation at wavelengths of 380 nm and 420 nm shows a relative lower activity below the baseline of the ultraviolet-visible absorption spectrum, these may result from the different light intensity by using the interference band-pass filters. Furthermore, a 24 h experiment with intermittent evacuation every 4 h under visible light (>420 nm) was performed to examine the stability of the CN-1.5 catalyst (Fig. 7b, inset). We find that CN-1.5 maintains most of its inherent photocatalytic reactivity without inactivation during six cycles, and the slight deactivation in photocatalytic activity may be due to the decreased concentration of TEOA which acts as the hole scavenger during the reaction [50].

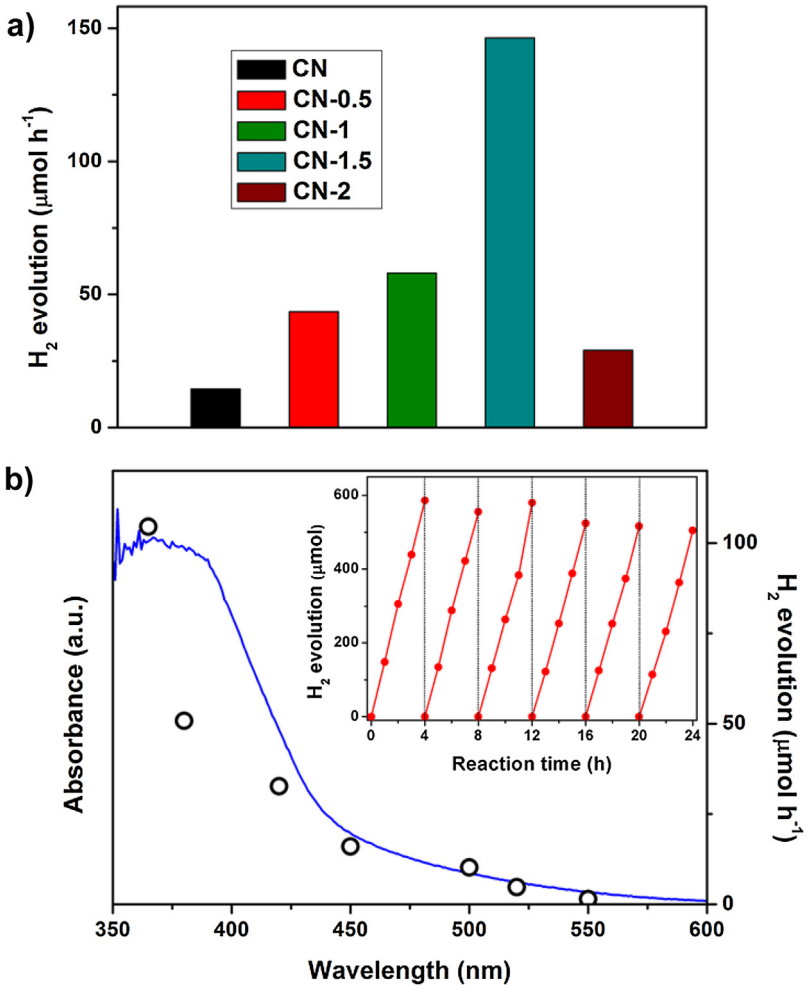

Fig. 7. (a) The rate of H_2 evolution on CN and CN-x samples under visible-light irradiation (($\lambda > 420$ nm). (b) Steady rate of H_2 production in aqueous triethanolaine solution (10 vol%) by 30 mg 3 wt% Pt-deposited CN-1.5 sample as a function of wavelength of the incident light. Ultraviolet–visible absorption spectrum of the catalyst is also shown for comparison. Inset is the stability test of the 3 wt% Pt-deposited CN-1.5 sample for H_2 production under visible light.

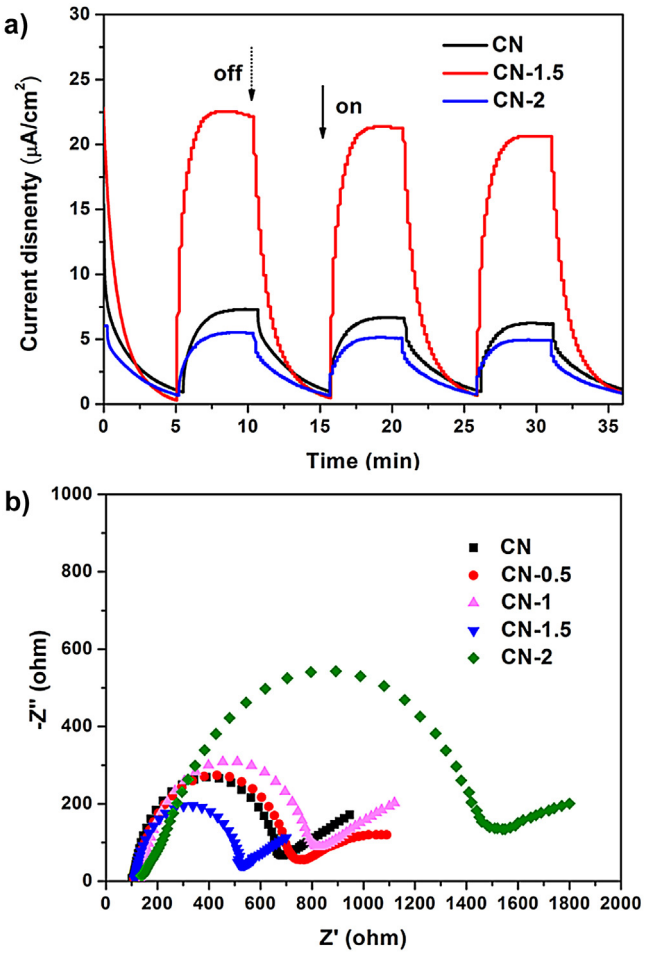

Fig. 8. (a) Transient photocurrent generation from CN, CN-1.5 and CN-2 electrodes at 0.6 V versus Ag/AgCl in 0.2 M Na_2SO_4 under simulated sunlight irradiation. (d) EIS Nyquist plots of CN, CN-1.5 and CN-2 samples.

Moreover, no CO_2 is formed during the whole photocatalytic hydrogen evolution reaction.

The photocurrent generation of the CN, CN-1.5 and CN-2 samples were investigated during ON/OFF illumination cycles at 0.6 eV. Looking at Fig. 8a, upon light irradiation, a typical *n*-type photocurrent was produced, suggesting the generation and separation of photoinduced $e^- - h^-$ pairs at CN/water interfaces. When the irradiation was interrupted, the photocurrent reverted to the original value once light was switched back on again. The transient photocurrent density of CN-1.5 is more than 20 $\mu A\,cm^{-2}$, whereas that of the CN and CN-2 is just about 7 $\mu A\,cm^{-2}$ and 5 $\mu A\,cm^{-2}$, respectively. The photocurrent decay of CN-2 indicates that the recombination processes are occurred seriously although it has a larger surface area, and the decay is largely determined by the efficiency of the transfer of conduction band electrons towards the back contact. On the contrary, as for the CN-1.5, the intrinsic drawback of fast charge recombination has been addressed, and a better photocatalytic performance can be expected.

To get further insight into the charge transport behavior in the CN samples, we investigated electrochemical impedance spectroscopy (EIS) measurements (Fig. 8b). To our knowledge, in the Nyquist diagram, the radius of each arc is associated with the charge-transfer process at the corresponding electrode/electrolyte interface with a smaller radius corresponding with a lower charge-transfer resistance. The CN-1.5 exhibits the smallest charge transfer resistance among all the CN samples, indicating the effective shuttling of charges between the electrode and the electrolyte, and a significantly improved electronic conductivity.

4. Conclusion

In conclusion, we successfully prepared a high-yield g-C_3N_4 with large surface area by in situ direct thermal condensation of cyanamide with the assist of the bifunctional urea. During the synthesis process of g-C_3N_4, urea may decompose into a lot of ammonia (NH_3) and carbon dioxide (CO_2), which serve as the nitrogen-source supply and the bubble-generating template respectively. The resultant g-C_3N_4 provides a large accessible surface area, and exhibits significantly improved performance for higher H_2 evolution rates together with the optical and electronic properties. The present synthesis route opened an avenue for the facile and economic preparation of high-yield g-C_3N_4-based materials with large surface areas, which would display wide practical applications in environmental remediation and energy transport.

Acknowledgements

This work was financially supported by National Natural Science Foundation of China (21573068 and 21603073), the Fundamental Research Funds for the Central Universities (WD1514303), SRF for ROCS, SEM, SRFDP, Program of Shanghai Subject Chief Scientist (15XD1501300) and China Postdoctoral Science Foundation Funded Project (2016M591615).

References

[1] J.E. Trancik, Nature 528 (2015) 333.
[2] P. Stott, Science 352 (2016) 1517–1518.
[3] D. Reay, Nature 538 (2016) 34–35.
[4] D.M. Kammen, D.A. Sunter, Science 352 (2016) 922–928.
[5] A. Kudo, Y. Miseki, Chem. Soc. Rev. 38 (2009) 253–278.
[6] X.L. Wang, W. Liu, Y.-Y. Yu, Y. Song, W.Q. Fang, D. Wei, X.-Q. Gong, Y.-F. Yao, H.G. Yang, Nat. Commun. 7 (2016) 11918–11924.
[7] A.Y. Meng, J. Zhang, D.F. Xu, B. Cheng, J.G. Yu, Appl. Catal. B: Environ. 198 (2016) 286–294.
[8] J.-D. Xiao, Q. Shang, Y. Xiong, Q. Zhang, Y. Luo, S.-H. Yu, H.-L. Jiang, Angew. Chem. Int. Ed. 55 (2016) 9389–9393.
[9] Y. Zhang, B. Ouyang, J. Xu, S. Chen, R.S. Rawat, H.J. Fan, Adv. Energy Mater. 6 (2016) 1600221.
[10] C. Liu, Z. Chen, Z. Wang, W. Li, E. Ju, Z. Yan, Z. Liu, J. Ren, X. Qu, Nanoscale 8 (2016) 12570–12578.
[11] X. Wang, K. Maeda, A. Thomas, K. Takanabe, G. Xin, J.M. Carlsson, K. Domen, M. Antonietti, Nat. Mater. 8 (2009) 76–80.
[12] S. Guo, Z. Deng, M. Li, B. Jiang, C. Tian, Q. Pan, H. Fu, Angew. Chem. Int. Ed. 55 (2015) 1830–1834.
[13] R.S. Sprick, J.-X. Jiang, B. Bonillo, S. Ren, T. Ratvijitvech, P. Guiglion, M.A. Zwijinenburg, D.J. Adams, A.I. Cooper, J. Am. Chem. Soc. 137 (2015) 3265–3270.
[14] J. Yan, H. Wu, H. Chen, L. Pang, Y. Zhang, R. Jiang, L. Li, S. Liu, Appl. Catal. B: Environ. 194 (2016) 74–83.
[15] X.L. Wang, W.Q. Fang, Y. Yao, P. Liu, Y. Wang, H. Zhang, H. Zhao, H.G. Yang, RSC Adv. 5 (2015) 21430.
[16] C. Liu, Z. Chen, Z. Wang, W. Li, E. Ju, Z. Yan, Z. Liu, J. Ren, X. Qu, Nanoscale 8 (2016) 12570–12578.
[17] Y. Zhang, B. Ouyang, J. Xu, S. Chen, R.S. Rawat, H.J. Fan, Adv. Energy Mater. 6 (2016) 1600221, http://dx.doi.org/10.1002/aenm.201600221.
[18] Y. Yuan, L. Zhang, J. Xing, M.I.B. Utama, X. Lu, K. Du, Y. Li, X. Hu, S. Wang, A. Genc, R. Dunin-Borkowski, J. Arbiol, Q. Xiong, Nanoscale 7 (2015) 12343–12350.
[19] X.L. Wang, W.Q. Fang, S. Yang, P. Liu, H. Zhao, H.G. Yang, RSC Adv. 4 (2014) 10676.
[20] Q. Liang, Z. Li, X. Yu, Z.-H. Huang, F. Kang, Q.-H. Yang, Adv. Mater. 27 (2015) 4634–4639.
[21] H. Li, L. Wang, Y. Liu, J. Lei, J. Zhang, Res. Chem. Intermed. 42 (2016) 3979.
[22] Y. Zheng, L. Lin, X. Ye, F. Guo, X. Wang, Angew. Chem. Int. Ed. 53 (2014) 11926–11930.
[23] Y. Zhao, F. Zhao, X. Wang, C. Xu, Z. Zhang, G. Shi, L. Qu, Angew. Chem. Int. Ed. 53 (2014) 13934–13939.
[24] G. Liu, P. Niu, C. Sun, S.C. Smith, Z. Chen, G.Q. Lu, H.-M. Cheng, J. Am. Chem. Soc. 132 (2010) 11642–11648.
[25] B. Yue, Q. Li, H. Iwai, T. Kako, J. Ye, Sci. Technol. Adv. Mater. 12 (2011) 034401.
[26] Y. Zhang, T. Mori, J. Ye, M. Antonietti, J. Am. Chem. Soc. 132 (2010) 6294–6295.

[27] T.Y. Ma, J. Ran, S. Dai, M. Jaroniec, S.Z. Qiao, Angew. Chem. Int. Ed. 54 (2015) 4646–4650.
[28] Y. Di, X. Wang, A. Thomas, M. Antonietti, ChemCatChem 2 (2010) 834–838.
[29] C. Han, L. Wu, L. Ge, Y. Li, Z. Zhao, Carbon 92 (2015) 31–40.
[30] J. Zhang, G. Zhang, X. Chen, S. Lin, L. Möhlmann, G. Dołęga, G. Lipner, M. Antonietti, S. Blechert, X. Wang, Angew. Chem. Int. Ed. 51 (2012) 3183–3187.
[31] G. Zhang, J. Zhang, M. Zhang, X. Wang, J. Mater. Chem. 22 (2012) 8083–8091.
[32] P. Niu, L.-C. Yin, Y.-Q. Yang, G. Liu, H.-M. Cheng, Adv. Mater. 26 (2014) 8046–8052.
[33] S. Yang, Y. Gong, J. Zhang, L. Zhan, L. Ma, Z. Fang, R. Vajtai, X. Wang, P.M. Ajayan, Adv. Mater. 25 (2013) 2452.
[34] J. Liu, T. Zhang, Z. Wang, G. Dawson, W. Chen, J. Mater. Chem. 21 (2011) 14398.
[35] Z. Lin, X. Wang, Angew. Chem. Int. Ed. 52 (2013) 1–5.
[36] K. Kailasam, A. Fischer, G. Zhang, J. Zhang, M. Schwarze, M. Schroder, X. Wang, R. Schomacker, A. Thomas, ChemSusChem 8 (2015) 1404–1410.
[37] Z. Yang, Y. Zhang, Z. Schnepp, J. Mater. Chem. A 3 (2015) 14081–14092.
[38] Y. Wang, M.F. Lbad, H. Kosslick, J. Harloff, T. Beweries, J. Radnik, A. Schulz, S. Tschierlei, S. Lochbrunner, X. Guo, Microporous Mesoporous Mater. 211 (2015) 182–191.
[39] J. Hong, X. Xia, Y. Wang, R. Xu, J. Mater. Chem. 22 (2012) 15006–15012.
[40] E. Ramasamy, C. Jo, A. Anthonysamy, I. Jeong, J.K. Kim, J. Lee, Chem. Mater. 24 (2012) 1575–1582.
[41] Y. Zhang, J. Liu, G. Wu, W. Chen, Nanoscale 4 (2014) 5300–5303.
[42] T. Steiner, Angew. Chem. Int. Ed. 41 (2002) 48–76.
[43] E. Arunan, G.R. Desiraju, R.A. Klein, J. Sadlej, S. Scheiner, I. Alkorta, D.C. Clary, R.H. Crabtree, J.J. Dannenberg, P. Hobza, H.G. Kjaergaard, A.C. Legon, B. Mennucci, D.J. Nesbitt, Pure Appl. Chem. 83 (2011) 1637–1641.
[44] X.L. Wang, W.Q. Fang, H.F. Wang, H. Zhang, H. Zhao, Y. Yao, H.G. Yang, J. Mater. Chem. A 1 (2013) 14089.
[45] Z. Yang, Y. Zhang, Z. Schnepp, J. Mater. Chem. A 3 (2015) 14081–14092.
[46] T. Sano, K. Koike, T. Hori, T. Hirakawa, Y. Ohko, K. Takeuchi, Appl. Catal. B: Environ. 198 (2016) 133–141.
[47] A. Thomas, A. Fischer, F. Goettmann, M. Antonietti, J.O. Mueller, R. Schloegl, J.M. Carlsson, J. Mater. Chem. 18 (2008) 4893–4908.
[48] X.L. Yang, F.F. Qian, G.J. Zou, M.L. Li, J.R. Lu, Y.M. Li, M.T. Bao, Appl. Catal. B: Environ. 193 (2016) 22–35.
[49] G. Zhang, J. Zhang, M. Zhang, X. Wang, J. Mater. Chem. 22 (2012) 8083–8091.
[50] L.J. Fang, X.L. Wang, Y.H. Li, P.F. Liu, Y.L. Wang, H.D. Zeng, H.G. Yang, Appl. Catal. B: Environ. 200 (2017) 578–584.